Available online at www.sciencedirect.com
ScienceDirect
Journal of Solid State Chemistry 180 (2007) 322–330
JOURNAL OF SOLID STATE CHEMISTRY
www.elsevier.com/locate/jssc

# Structural characterization of the hollandite host lattice for the confinement of radioactive cesium: Quantification of the amorphous phase taking into account the incommensurate modulated character of the crystallized part

A.Y. Leinekugel-le-Cocq-Errien[a], P. Deniard[a,*], S. Jobic[a], E. Gautier[a], M. Evain[a], V. Aubin[b], F. Bart[c]

[a]*Institut des Matériaux Jean Rouxel, UMR 6502, CNRS-Université de Nantes, Laboratoire de Chimie des Solides, 2 rue de la Houssinière, BP32229, 44322 Nantes cedex 3, France*
[b]*LCAES-ENSCP 11 rue Pierre et Marie Curie, 75231 Paris cedex 05, France*
[c]*CEA Valrhô Marcoule, DEN-DTCD-SECM, Laboratoire d'Etude des Matériaux Céramiques pour le Conditionnement BP 17171 30207 Bagnols sur Ceze cedex, France*

Received 12 June 2006; received in revised form 9 October 2006; accepted 10 October 2006
Available online 21 October 2006

**Abstract**

X-ray patterns of the $Ba_1Cs_{0.28}Fe_{0.82}Al_{1.46}Ti_{5.72}O_{16}$ compound evidence two wide peaks at low angle in addition to the well defined peaks of the $I4/m$ hollandite structure type. Two hypotheses have been explored to account for these features: the coexistence of the hollandite phase with an amorphous phase and the appearance of a commensurate or incommensurate modulated structure associated with a cationic ordering, as proposed in the literature. Actually, even if the amorphous phase quantification by the Rietveld method reveals about 15 wt% of non-crystalline phase in some of the powdered sample, the origin of the two wide peaks was found to stem from the incommensurate modulated character of the hollandite structure type (super space group $I4/m(0\,0\,\gamma)0\,0$) with a distribution of the modulation wavevectors presumably related to slight chemical composition changes.


*Keywords:* XRD; Amorphous phase quantification; Incommensurate modulated structure; Nuclear waste confinement

## 1. Introduction

Concomitantly to the perpetual, growing race to the nuclear energy to generate electricity (currently, about 17% of the electricity world production stems from nuclear plants), the nuclear waste conditioning becomes a crucial problem to address in the coming years. Cesium is one of the principal fission radionuclides resulting from the reprocessing of spent nuclear fuel. This element turns out to be very difficult to immobilize because of its high volatility and its ability to form water soluble compounds. Moreover, $^{134}Cs$ and $^{137}Cs$ isotopes with high calorific power ($4.8\times10^{13}$ and $4.3\times10^{7}$ Bq/g, respectively) and $^{135}Cs$ with a $2.3\times10^{6}$ years half-life increase the difficulty of its conditioning.

To specifically immobilize cesium, the $Ba_1Cs_{0.28}Fe_{0.82}Al_{1.46}Ti_{5.72}O_{16}$ material with a hollandite structure was proposed by CEA [1]. The chosen chemical composition results from successive Cs concentration optimization steps taking into account the Cs heat generating capacity and the transmutation of $Cs^+$ into $Ba^{2+}$. It was designed at the time of the Synroc study (SYNthetic ROCk), a synthetic mineral originally developed for the immobilization of nuclear high-level wastes (i.e. radionuclides with an activity around $10^9$ Bq/g) issued from nuclear reactor fuel [2,3], and consisted of an assembling of perovskite ($CaTiO_3$), zirconolite ($CaZrTi_2O_7$), hollandite ($Ba_xAl_{2x}Ti_{8-2x}O_{16}$)

*Corresponding author. Fax: +33 2 40 37 39 95.
*E-mail address:* philippe.deniard@cnrs-imn.fr (P. Deniard).

0022-4596/$ - see front matter © 2006 Elsevier Inc. All rights reserved.
doi:10.1016/j.jssc.2006.10.013

which could also contain inert materials such as rutile, zircone or alumina. Hollandite acted as the host for radioactive cesium, barium and other large alkali ions as Rb.

The objective of reported experimental study is to perfectly characterize the structure of the $Ba_1Cs_{0.28}Fe_{0.82}Al_{1.46}Ti_{5.72}O_{16}$ hollandite batches to explain on the one hand its high lixiviation performance and to give, on the other hand, an accurate structure determination for further thermodynamical characterization of its long life behavior.

## 2. Experimental section

### 2.1. Synthesis

Hollandite specimens named hereafter *ha* are synthesized by the alcoxyde route and those named *hd* are obtained by the dry method, described in a previous paper [4]. The alcoxyde route uses titanium and aluminum alcoxyde, iron, barium, and cesium nitrates as precursors and the dry route cesium, iron, and aluminum nitrates, barium carbonate, and anatase. Specimens under discussion hereafter, whatever the synthesis route, are obtained after a two-step procedure: a calcination at 1000 °C (3 h for *ha*, 6 h for *hd*) and a subsequent sintering at 1200 °C after a 120 MPa pressure step at room temperature.

### 2.2. Characterization

*XRD.* X-ray diffraction (XRD) was run using two different Siemens D5000 diffractometers in a Bragg-Brentano geometry with a copper anode (Cu$K$-$L_{3,2}$, $\lambda = 1.540598$ and 1.544390 Å) at a controlled temperature of 293 K. The first experiment done in a routine way, prior to any amorphous phase quantification, was done with an Elphys linear detector that presents the advantage of a fast data collection with the drawback of a poor signal over background ratio. All the subsequent experiments were carried out using a second diffractometer equipped with a Moxtek punctual detector. The first data collection was done on the as received hollandite pellet obtained after the as above-mentioned sintering step. For phase quantification, the powder (hollandite/anatase mixture) was placed on a plate with circular recess and scraped flush with the surface using a ground glass slide to minimize any preferred crystallite orientation. The plate was then positioned so that the sample surface was perfectly flat and tangential to the goniometer focusing circle. Patterns were collected from 15° to 115° in 2$\theta$ with a 0.025° 2$\theta$ step. Structure analysis via Rietveld refinements were performed with the Fullprof2000 program [5]. The Rietveld refinement strategy used for all the data consisted in a background refinement using a six term polynomial, a simple pseudo-Voigt for the line profile, a March Dollas preferred orientation correction only for the pellet sample (any attempt to refine this parameter for powdered material led to a value close to zero within the standard uncertainty), no asymmetry corrections were necessary as no important Bragg peaks are found below 28° 2$\theta$. For all the patterns, a sample height correction parameter was refined. For all the refinements, the correlation between atomic displacement parameter and site occupancy, that could be important, was checked through the observation of the correlation matrix. It was also verified that, for a given atom, the couple of values for these two parameters did not change within standard uncertainty from one cycle to the other. In addition, the site occupation fraction of Ba and Cs was compared to the expected value deduced from the chemical analysis and always found to be in very good agreement within standard uncertainty. The site occupation fraction of titanium, aluminum and iron was fixed to the expected value from sample preparation, as these three elements are located in the same crystallographic position.

*Amorphous quantification by Rietveld method:* An XRD quantification of an amorphous phase was systematically done. Formally, Rietveld method can be used to quantify an amorphous phase [6] (i.e., a true amorphous phase or a crystalline phase with crystallite sizes not large enough to give rise to Bragg peaks), using an internal standard with a well known weight percentage. In the present case, 50 wt% of our sample was intimately mixed in an agate mortar with 50 wt% of anatase (Merck purity >99.0%). The choice of this standard is based upon the fact that the anatase is perfectly characterized and does not evidence too many diffraction peaks overlapping those of the $Ba_1Cs_{0.28}Fe_{0.82}Al_{1.46}Ti_{5.72}O_{16}$ hollandite compound. The percentages obtained by the Rietveld analysis, which quantifies only crystallized phases, does not take into account an eventual amorphous phase. Therefore, the standard, anatase here, is used as a weight reference to readjust the percentages and quantify the amorphous phase from the difference between 100% and the percentage of crystallized phases [7]. The percentage of the latter, as obtained by the Rietveld method depends, however, on the X-ray microabsorption contrast (linear absorption and particle sizes of all the phases in the sample). Thus, to access the actual percentages, absorption contrast Brindley's factors were considered [8] and calculated, taking into account the particle sizes issued from laser diffraction particle size and scanning electron microscope (SEM) high resolution analyses.

*SEM:* Ultimate analyses have been done on our samples by energy-dispersive X-ray spectroscopy (EDXS) on a SEM JEOL 5800 at 10 keV to determine the Cs/Ba ratio. Samples were pelletized ($\phi = 13$ mm, under 250 MPa) to minimize roughness-related errors. Oxygen content was not probed and the iron, titanium, and aluminum stoechiometric coefficients were normalized with the sum rule Fe + Al + Ti = 8. The chemical composition obtained for the sintered samples (*ha* and *hd* specimens) was "$Ba_{1.3}Cs_{0.3}Fe_{0.8}Al_{1.3}Ti_{5.9}O_{16}$" (average from 14 analyses), in good agreement with the $Ba_1Cs_{0.28}Fe_{0.82}Al_{1.46}Ti_{5.72}O_{16}$ expected composition. High resolution images on SEM were

collected on a JEOL JSM 6400F equipped with a field emission gun.

*Laser diffraction particle size analysis:* Laser particle size analysis was performed with a Beckman Counter LS230 with powders dispersed in permuted water with sodium hexametaphosphate as surfactant.

*MET:* Electron diffraction (ED) as EDXS analysis was carried out on a Philips-CM30 microscope at 300 kV. Polycrystalline ceramic fragments were ground in ethanol and dispersed onto holey carbonaceous support films of polymers. JEMS program [9] was used for indexing electron diffraction pattern. EDXS was done with the Link ISIS 3.32 software, 1992–1997, Oxford Instruments plc. High Resolution Electron Microscopy (HREM) was carried on a Hitachi HNAR 9000 at 300 kV.

## 3. Results and discussion

The structure of hollandite, with the general formula $A_xB_8O_{16}$ ($x \leqslant 2$), consists of double rutile chains built from $BO_6$ edges- and corners-sharing octahedra which form tunnels along the *c*-axis where $A^+$ or $A^{2+}$ cations are located (Fig. 1). The symmetry can be tetragonal ($I4/m$) or monoclinic ($I2/m$) according to the nature and the amount of the *A* counter-ion [10–13]. The symmetry of the hollandite is usually tetragonal in presence of cesium in the tunnel, even in very small quantities [14]. When the *A* site is only partially occupied, an ordering between atoms and vacancies may induce a superstructure [15,16].

Our Rietveld refinements on the as obtained *ha* hollandite (raw pellet from sintering) led to the structural results already published [4]. As barium and cesium cannot be distinguished by lab XRD at the Cu-$L_{2,3}$ radiation wavelength, only the mean atomic position of the *A* site was refined. As mentioned above a preferred orientation factor of 0.962(3) using the March–Dollas model has been necessary in this refinement. This is probably due to the pressure effect of sintering.

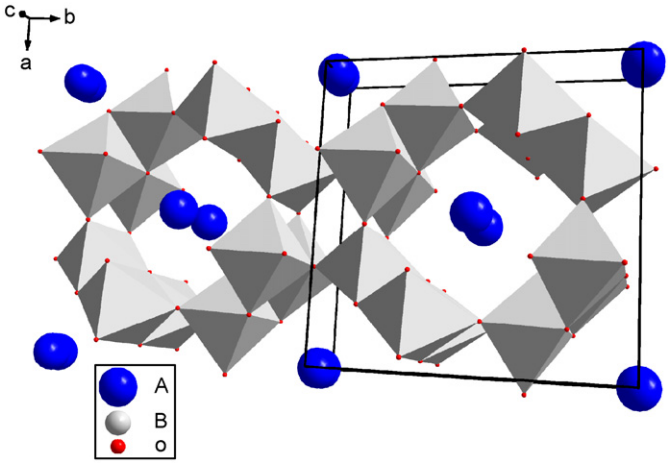


Fig. 1. Tetragonal $A_xB_8O_{16}$ hollandite structure representation along the *c*-axis.

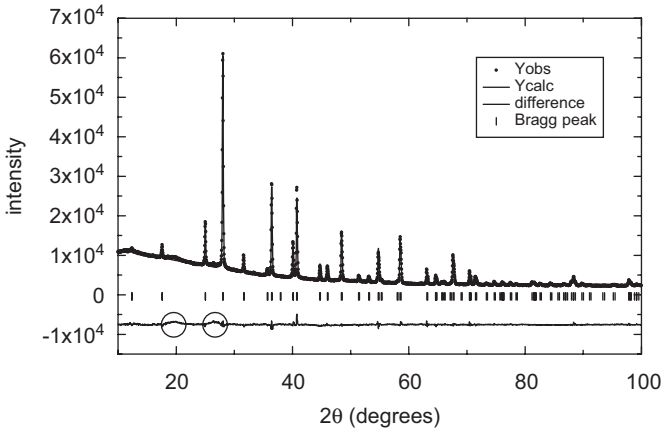


Fig. 2. Observed, calculated, and difference X-ray diffraction pattern of *ha* sintered hollandite after refinement. Notice the two broad peaks at low angles.

In our previous paper [4], the occurrence of two low angle broad peaks in addition to the basic structure (Fig. 2) was not discussed. To explain their occurrence, the first interpretation is naturally the possible presence of an amorphous phase, even if preliminary investigations by Cheary et al. concluded to a superstructure in a $Ba_x(Mg_{1-x}Ti_8)O_{16}$ hollandite [17], although the latter interpretation would in principle induce the rising up of well defined sharp peaks instead of wide bumps as observed. In the same way, Carter and Withers [13] reported the same superstructure interpretation based on the occurrence of a superstructure in a hollandite material with a composition closer to that we study ($Ba_x(Fe_xTi_{8-x})O_{16}$ with $1 \leqslant x \leqslant 1.4$). As the assumption of the existence of an amorphous phase had not been considered, we have to try to see whether, it could not give rise to broad peaks, fortuitously localized at the same angular positions as the Bragg peaks related to a superstructure.

### 3.1. The amorphous phase

From laser diffractometry, it appears that anatase particles follow a bimodal size distribution around 0.5 and 2 μm. In contrast, sintered *ha and hd* hollandite specimens, obtained after a mixing with anatase before the amorphous quantification by DRX, highlighted three types of particles with diameters peaking at about 0.5, 2 and 4 μm, respectively (see Fig. 3).

Pure anatase has also been observed by SEM (Fig. 4). It appears only as a very fine, mono-dispersed powder with particle size lower than 0.5 μm. The discrepancy with the laser diffractometry results probably originates from the propensity of the $TiO_2$ particles to agglomerate. To correctly calculate the absorption of each component and get an accurate amorphous quantification through Brindley's corrections, particle sizes were taken at 0.5 μm for anatase and 2 or 4 μm for hollandite.

After the particle size measurements, the anatase–hollandite mixture has been studied by XRD to obtain

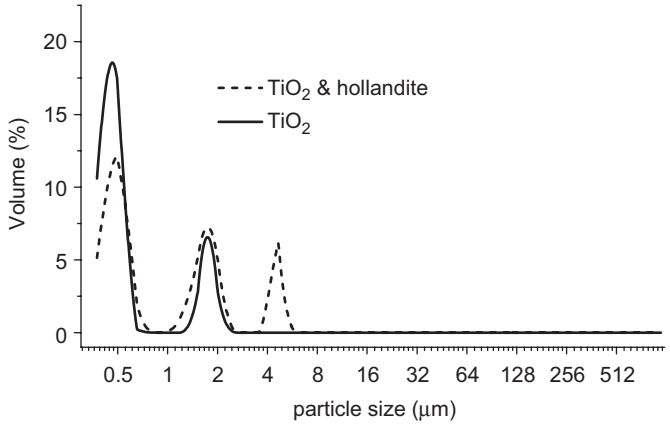


Fig. 3. Laser particle size analysis on the pure anatase and its mixture with hollandite.

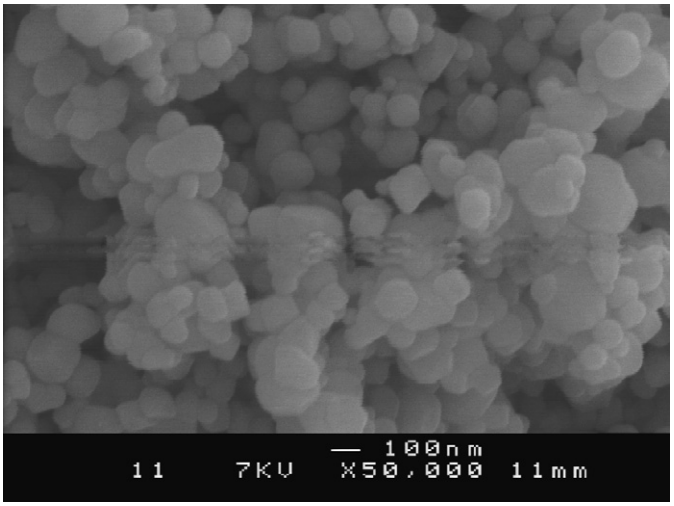


Fig. 4. Observation of anatase particle size by SEM.

the percentages of the crystallized phases, without any absorption correction. For the *ha* hollandite compound, refinement results are gathered in Table 1 and XRD patterns are given in Fig. 5. Cell parameters, here obtained on *ha* powders, are a little bit larger than those we previously reported on ha pellets. This can be attributed to a lower cesium content on the pellet surface as compared to the bulk, in agreement with a Time-of-Flight Secondary Ion Mass Spectroscopy study [18] indicating a cesium depletion in the extreme outer surface of the sample (to a depth of 1–2 μm). This depth matches well the penetration depth of Cu$K$-$L_{2,3}$ X-ray beam calculated with the Bruker Diffrac-Plus package (90% of the analyzed material is located in the first 3 μm at an incident beam angle of 30° $2\theta$). This effect of composition on cell parameters is more sensitive than the Ba/Cs site occupation fraction that is found to be equal in both cases, within standard uncertainties. Structural refinement results were found to be identical, within standard uncertainties, for *hd* and *ha* hollandite.

Results of the amorphous quantification for *ha* compounds, obtained after the readjustment following the anatase addition and the Brindley's absorption corrections, are presented in Table 2. As the method sensitivity is about 3 wt% [8], it can be concluded that an amorphous phase does exist in the sample and is quantified at about 10 wt% (average of values depending on particle size attribution). Any attempt to locate this amorphous phase as an isolated material in the preparation, using TEM (SAED and HREM), was unsuccessful and led us to think that it was located around the crystallized hollandite itself as a coating. Notice that the EDXS measurements, coupled with HREM, did not give any composition difference between the crystal bulk and its border, indicating that the amorphous phase should have a composition very similar to that of the main phase (i.e., $Ba_1Cs_{0.28}Fe_{0.82}Al_{1.46}Ti_{5.72}O_{16}$).

The amorphous layer thickness has been evaluated as following: If one considers, as mentioned above, that this phase has a composition close to that of the crystallized hollandite, its density must be also very similar. Hence, the amorphous phase percentage is directly proportional to the volume of each phase and the thickness calculation of this amorphous phase is very simple if one considers, in a first approach, a spherical crystal covered with an amorphous layer: $\%_{amorphous} = (r^3-(r-x)^3)/r^3$ with $r$ the total particle radius and $x$ the amorphous layer thickness.

For an amorphous phase weight percentage of 12%, the amorphous phase thickness should be around 410 Å in the case of hollandite crystals which are 2 μm in diameter, and 830 Å for 4 μm hollandite particles. Such a thickness should make possible the detection of the amorphous phase by TEM. As this is not the case, the simple coating hypothesis was rejected.

The other possibility is that the amorphous phase is located not around the crystals but around the crystallites themselves (Fig. 6). To explore this possibility, crystallite size needs to be determined. This can be done from XRD measurements since the crystallite size has a direct incidence on the peak width, which is also influenced by an instrumental contribution. To deconvoluate the peaks, the fundamental parameter approach [19,20] (profile convolution representing the equipment contribution on peak profiles) was applied on the X-ray powder pattern using the XFIT program [21] to model the instrumental resolution and make possible the deduction of the crystallite size. With this experimental approach, the hollandite crystallite size was estimated around 0.2 μm. Consequently, the thickness of the amorphous coating around the crystallite crust should be around 41 Å which is realistic. To locate the amorphous phase, high resolution images were performed.

By HREM, crystals are observed without any amorphous phase at their border (Fig. 7). This can be due to the fact that the observed border area corresponds to a broken crystallite obtained from the sintered material during grinding or to a dissolution of the amorphous phase in

Table 1
Rietveld refinement results of a *ha* hollandite/anatase mixture for amorphous phase quantification

| Phase 1 | Space group | | Cell parameters (Å) | | | |
|---|---|---|---|---|---|---|
| *ha* | *I*4/*m* | | *a* 10.0480(2) | | *c* 2.94246(11) | |
| Atoms | Site | *x* | *y* | *z* | *U* | Occupation |
| Ba/Cs | 4*e* | 0 | 0 | 0.623(2) | 0.006 | 0.30(1) |
| Ti | 8*h* | 0.3505(5) | 0.1669(6) | 0 | 0.013 | 0.714 |
| Al | 8*h* | 0.3505 | 0.1669 | 0 | 0.013 | 0.182 |
| Fe | 8*h* | 0.3505 | 0.1669 | 0 | 0.013 | 0.102 |
| O1 | 8*h* | 0.1599(14) | 0.2036(14) | 0 | 0.013 | 1 |
| O2 | 8*h* | 0.5504(14) | 0.1650(15) | 0 | 0.013 | 1 |
| $R_{Bragg} = 9.53$ | | | 45.4(6) wt% | | | |

| Phase 2 | Space group | | Cell parameters (Å) | | | |
|---|---|---|---|---|---|---|
| Anatase | *I*41/*amd* | | *a* *3.78465(7)* | | *c* *9.5123(2)* | |
| Atoms | Site | *x* | *y* | *z* | *U* | Occupation |
| Ti1 | 4*a* | 0 | 0.25 | 0.375 | 0.008 | 1 |
| O1 | 8*e* | 0 | 0.25 | 0.1667(4) | 0.013 | 1 |
| $R_{Bragg} = 4.63$ | | | 54.6(5) wt% | | | |
| $R_p = 12.4$ | $R_{wp} = 17.7$ | $R_{exp} = 10.60$ | $\chi^2 = 2.78$ | | | |

Percentages obtained here are rough, without taking into account the eventual amorphous phase.

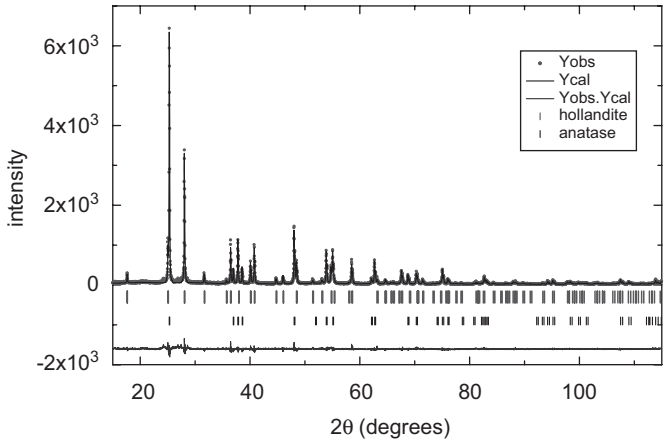


Fig. 5. Observed, calculated, and difference X-ray diffraction pattern of *ha* sintered hollandite mixed with pure anatase for amorphous phase quantification.

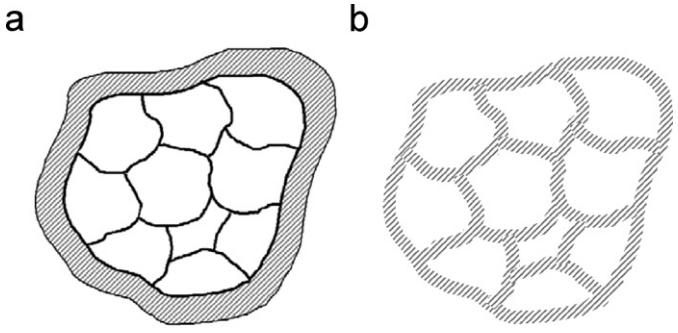


Fig. 6. Schematic representation of an amorphous coating around (a) a crystal made of crystallites and (b) around the crystallites themselves.

Table 2
Amorphous quantification on *ha* sintered hollandite

| Particle size (μm) | | wt% of amorphous phase |
|---|---|---|
| Anatase | Sintered hollandite | |
| 0.5 | 2 | 12 |
| 0.5 | 4 | 9 |

the ethanol used for the TEM grid preparation (this has to be considered for an amorphous phase with a structure different from hollandite). The observation gives also another piece of information: the hollandite degradation under the electron beam is slow which indicates that, if an amorphous phase can be seen, there is a good chance it does not come from material amorphization under the electron beam. On the same image, we observe an apparently amorphous grain boundary between two crystallites. Its thickness is determined around 11 Å. This is lower than the expected value (41 Å). This appearing discrepancy may be due to an amorphous phase having a density slightly different than that of $Ba_1Cs_{0.28}Fe_{0.82}Al_{1.46}$

$Ti_{5.72}O_{16}$ itself, leading to a small change in the phase quantification. However, the order of magnitude is correct since 41 Å is only an average value. Therefore, an amorphous phase is present and is located at the crystallite periphery in *ha* sample (obtained by the alcoxyde route).

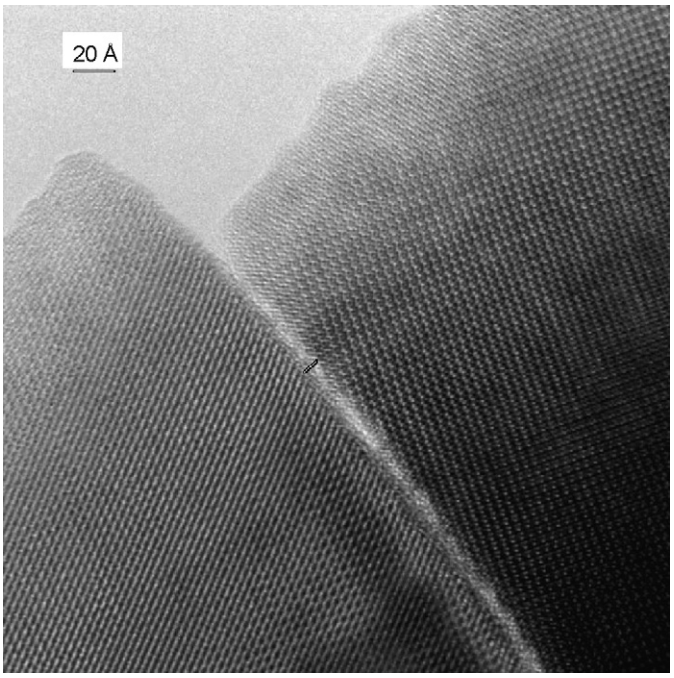


Fig. 7. High-resolution images along the [1 0 0] zone axis. Note the crystalline character of the compound in the border area and the amorphous grain boundary between two crystals with a thickness estimated around 11 Å.

In contrast, *hd* sample (obtained by the dry route) gives different results. Whatever the anatase and hollandite particle sizes, the crystallized phase percentages, obtained after Brindley's corrections applied on XRD refinement (see Table 3 for results), lead to a negative percentage (−8.5 wt%) of amorphous phase in this sample. This is the clear indication that some parameters are not taking into account in the amorphous phase quantification procedure leading to an under estimation. This point will be discussed below. In a first step, let's consider that the *hd* sample does not contain any amorphous phase that is the minimum value one can physically accept. Nevertheless, its XRD powder pattern presents the two broad peaks mentioned above. Thus, those peaks cannot be due to an amorphous phase whatever the chosen synthesis route.

### 3.2. The modulated structure

If the broad peaks are not due to the amorphous phase, the modulated structure hypothesis has to be considered. To check the possibility of an aperiodicity, we reinvestigated the crystal structure of hollandite of the simplified ($Ba_{1.16}Al_{2.32}Ti_{5.68}O_{16}$) formulation on single crystal [22] and on the corresponding powder. The single crystal refinement highlights the existence of an incommensurate structure implying displacive and occupation modulations of Ba along the *c*-axis (super space group: $I4/m(0\,0\,\gamma)0\,0$).

Table 3
Rietveld refinement results of a *hd* hollandite/anatase mixture for amorphous phase quantification

| Phase 1 | Space group | | Cell parameters (Å) | | | |
|---|---|---|---|---|---|---|
| *hd* | *I*4/*m* | | *a* 10.0503(2) | | *c* 2.94494(12) | |
| Atoms | Site | *x* | *y* | *Z* | *U* | Occupation |
| Ba/Cs | 4*e* | 0 | 0 | 0.6306(18) | 0.006 | 0.30(1) |
| Ti | 8*h* | 0.3508(4) | 0.1662(5) | 0 | 0.013 | 0.714 |
| Al | 8*h* | 0.3508 | 0.1662 | 0 | 0.013 | 0.182 |
| Fe | 8*h* | 0.3508 | 0.1662 | 0 | 0.013 | 0.102 |
| O1 | 8*h* | 0.1515(11) | 0.2028(11) | 0 | 0.013 | 1 |
| O2 | 8*h* | 0.5452(11) | 0.1659(12) | 0 | 0.013 | 1 |
| $R_{Bragg} = 8.48$ | | | 47.2(5) wt% | | | |

| Phase 2 | Space group | | Cell parameters (Å) | | | |
|---|---|---|---|---|---|---|
| Anatase | *I*41/*amd* | | *a* 3.78500(7) | | *c* 9.5133(2) | |
| Atoms | Site | *x* | *y* | *Z* | *U* | Occupation |
| Ti1 | 4*a* | 0 | 0.25 | 0.375 | 0.007 | 0.25 |
| O1 | 8*e* | 0 | 0.25 | 0.1663(3) | 0.013 | 0.125 |
| $R_{Bragg} = 8.69$ | | | 52.8(4) wt% | | | |
| $R_p = 10.1$ | $R_{wp} = 13.2$ | $R_{exp} = 7.85$ | $\chi^2 = 2.82$ | | | |

Percentages obtained here are rough, without taking into account the eventual amorphous phase.

On two single crystals from the same preparation, two different modulation wavevectors were refined, i.e., $\mathbf{q} = 0.38\,\mathbf{c}^*$ or $0.40\,\mathbf{c}^*$. The corresponding calculated powder pattern presents sharp peaks exactly at the same positions as those of the two broad peaks on the observed pattern. The widening of the peaks can be explained by a distribution of modulation wavevectors ranging from $\mathbf{q} = 0.36$ to $0.44\,\mathbf{c}^*$ associated to a modification of the structure arrangement (mainly due to an occupancy modulation) (Fig. 8).

The same treatment applied to *ha* and *hd* $Ba_1Cs_{0.28}Fe_{0.82}Al_{1.46}Ti_{5.72}O_{16}$ samples can explain the two broad peaks with a **q** wavevector distribution ranging from $\mathbf{q} = 0.30$ to $0.48\,\mathbf{c}^*$ (Fig. 9). This **q** wavevector distribution was estimated assuming Dirac-like peaks for each **q** wavevector value in such a way to frame the observed peak. Thus the as determined range is overestimated since the peaks must have an intrinsic width due to coherence length along the tunnels.

Those results are in good agreement with Mijhloff et al. [23], Zandbergen et al. [24] and Kesson and White [25,26] studies. In the related papers, a correlation was established between the $x$ tunnel-site occupancy and the $m$ multiplicity of the modulated structure defined as $d_{\text{supercell}}$ divided by $d_{002}$ for the subcell: $1/2x = 1-(2/m)$. In our case, assuming this equation, $m$ was estimated to be equal to 5.55. The relation between the **q** modulation wavevector and the multiplicity $m$ is: $m = 2/\mathbf{q}$. Then, with the experimental results and assuming a mean **q** wavevector value of $0.39\,\mathbf{c}^*$, the corresponding multiplicity is 5.42, value very similar to that found in the literature.

To confirm those results, electron diffraction has been done on sintered hollandite.

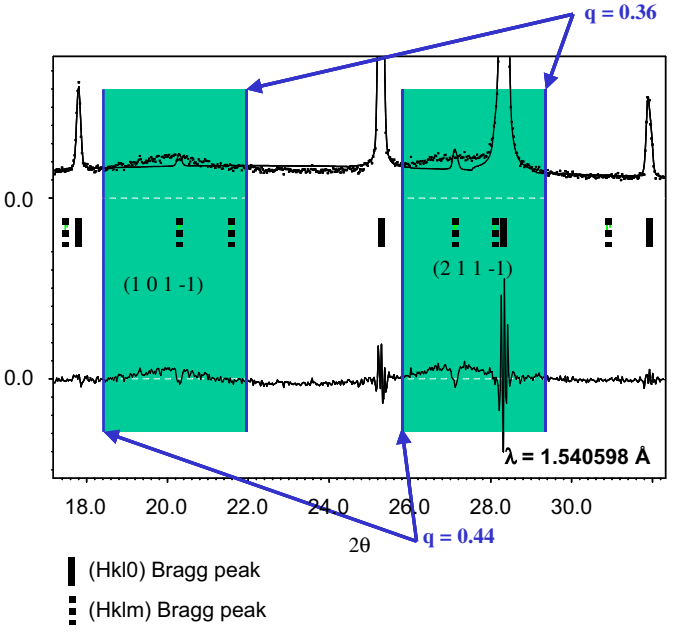


Fig. 8. Explanation of the two wide peaks on powder diffraction pattern of $Ba_{1.16}Al_{2.32}Ti_{5.68}O_{16}$ sample with a modulation wavevector distribution ranging from 0.36 to $0.44\,\mathbf{c}^*$.

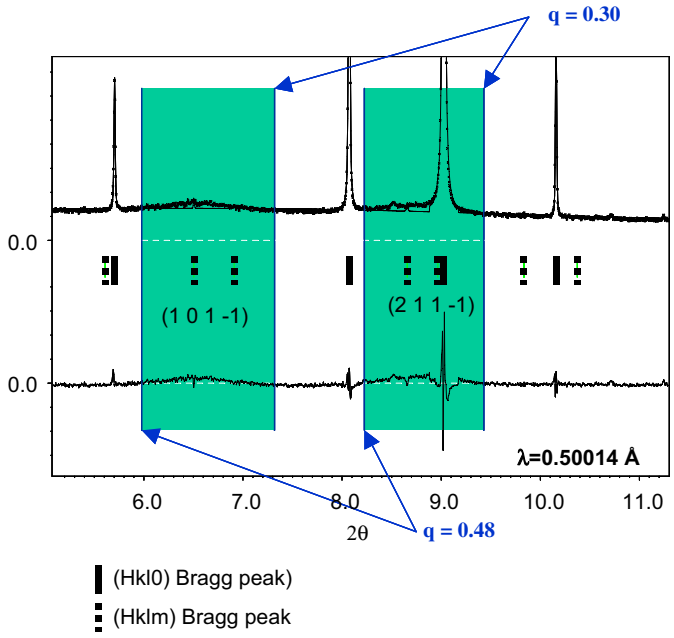


Fig. 9. Explanation of the two wide peaks on powder diffraction pattern of $Ba_1Cs_{0.28}Fe_{0.82}Al_{1.46}Ti_{5.72}O_{16}$ (*ha*) sample with a modulation wavevector distribution ranging from 0.30 to $0.48\,\mathbf{c}^*$.

Fig. 10 shows the electron diffraction pattern (EDP) taken from the hollandite $Ba_1Cs_{0.28}Fe_{0.82}Al_{1.46}Ti_{5.72}O_{16}$ along the [1 0 0] zone axis. The satellite spots produced by the modulation can be seen on this pattern along $\mathbf{c}^*$. The **q** wavevector is estimated to be $0.378 + 0.002\,\mathbf{c}^*$ (averaged from five measurements).

Another crystal of the same batch shows again satellite spots due to the modulation along the [1 1 1] zone axis (Fig. 11). This time, the estimation of the modulation wavevector gives $0.429 + 0.004\,\mathbf{c}^*$ (averaged from five graphic measurements).

Those two different modulation wavevectors obtained on two different crystals of the same batch confirm the presence of the modulated structure in our materials and prove that the broad peaks on powder X-ray diffraction pattern arise from a distribution of **q** wavevectors. The two different crystals present a slight difference of composition: from microprobe analysis, composition was found to be $Ba_{1.28}Fe_{0.92}Al_{1.64}Ti_{5.44}O_{16}$ for $\mathbf{q} = 0.364\,\mathbf{c}^*$ modulation wavevector and $Ba_{1.32}Fe_{1.28}Al_{0.96}Ti_{5.66}O_{16}$ for $q = 0.376\,\mathbf{c}^*$. Therefore, the distribution of modulation wavevectors seems to be due to a small local difference of composition that can be observed neither by EDXS on SEM nor by TEM. These results are in a good agreement with those of Carter and Withers [13] who reported a shift in satellite peak positions as a function of $x$ in $Ba_xFe_xTi_{8-x}O_{16}$.

### 3.3. Combining the amorphous phase quantification and the modulated structure

During the Rietveld procedure, it was not possible to take into account the incommensurate modulation

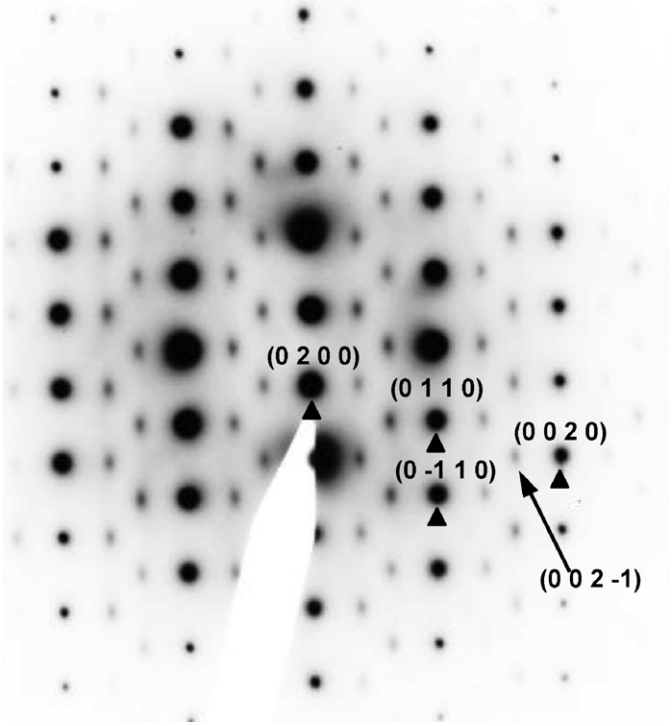


Fig. 10. EDP taken from an hollandite crystal along the [1 0 0] zone axis showing satellite spots with a $\mathbf{q} = 0.378\,\mathbf{c}^*$ modulation wavevector. The extinction conditions in the $I4/m(0\,0\,\gamma)0\,0$ superspace group are: $h+k+1 = 2n+1$.

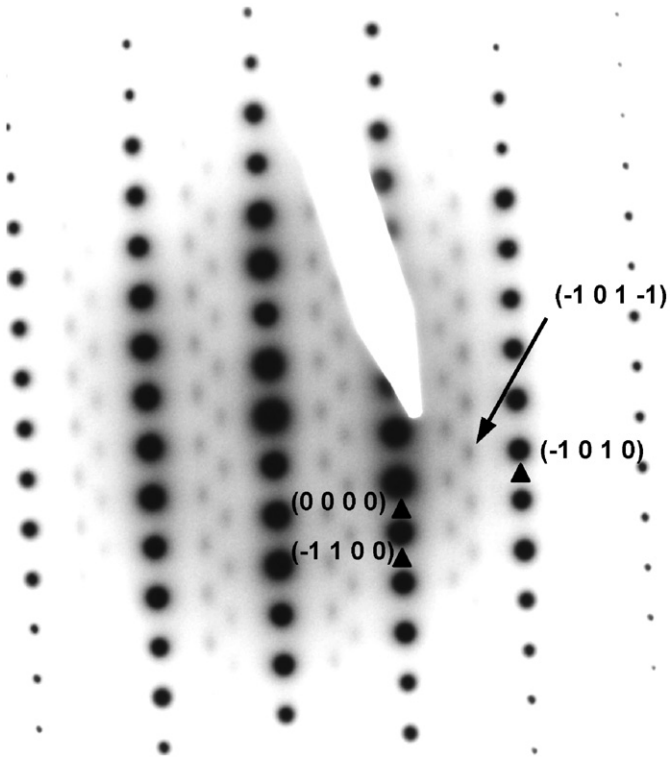


Fig. 11. EDP taken from an hollandite crystal along the [1 1 1] zone axis showing satellite spots with a $\mathbf{q} = 0.429\,\mathbf{c}^*$ modulation wavevector (owing to their out of plane location, satellites spots have a weaker intensity than in Fig. 10).

character of the hollandite material, because of its too tiny signature on the diffraction pattern (moreover, the distribution of wavevectors in the powder leads to a widening of these modulation peaks and thus to a lowering of their count number). Hence, this leads to an error in the hollandite scale factor refined in the Rietveld technique, this factor being at the root of the phase quantification. Indeed, a part of the base structure intensity is distributed in the satellite peaks. As the intensities of the latter are not taking into account in the calculation, the scale factor is over estimated to allow the calculated pattern to match the observed one. As a consequence, the percentage of crystallized hollandite phase is over estimated, leading to an under estimation of a potential amorphous phase. To try to estimate the scale factor error and being unable to calculate the satellites intensities in the powder diffraction pattern, we have considered that their percentage, compared to that of the main diffraction peaks, was about the same as in the single crystal experiment based on a similar material [22]. The ratio $\sum I_{h,k,l,m=1 \text{ or } 2} / \sum I_{h,k,l,m=0}$ was found to be equal to 0.08. Thus the scale factor, as determined from Rietveld refinement, has been decreased by 8%. As a result, the *ha* material does not contain 8.6% of amorphous phase but 14.5%. As for *hd* compound, its amorphous phase percentage increases from −8.55 to −1.65, value that can be considered equal to zero, taking into account the technique sensitivity estimated to be around ±3%. One can notice that as the phase percentage calculation is only based on the scale factor $S$, the number of formula units $Z$, the cell volume $V$ and, the mass of the formula unit $m$, the non-consideration of satellite intensities should lead to an amorphous phase quantity equal to the scale factor error ($Z$, $V$, and $m$ referring to the same material). It's about what is observed in our calculation since the amorphous phase quantification varies from −8% to zero, within the errors. These errors come from the use of an intensity correction based on a single crystal study of a slightly different composition, these correction depending on the maximum order of the satellites used for the calculation (here limited to two).

## 4. Conclusion

The hollandite under study with a $Ba_1Cs_{0.28}Fe_{0.82}Al_{1.46}Ti_{5.72}O_{16}$ composition can be obtained by an alcoxyde or a dry route. It presents a tetragonal space group ($I4/m$). *ha* sample contains an amorphous phase quantified by Rietveld method at about 14.5 wt%. This amorphous phase is supposed to be localized at the crystallite borders. The same study on *hd* sample shows no amorphous phase although wide peaks on XRD powder patterns are observed. This indicates that, even if an amorphous phase may exist in some compounds, it is not responsible for the occurrence of the low angle broad peaks. Thanks to a single crystal study of a simplified hollandite $Ba_{1.16}Al_{2.32}Ti_{5.68}O_{16}$, an incommensurable modulated structure with the $I4/m(0\,0\,\gamma)0\,0$ super space group was evidenced. The

consideration of this modulated structure to our sample explains wide peaks on XRD powder patterns with a **q** wavevector distribution ranging from $\mathbf{q} = 0.30\,\mathbf{c}^*$ to $\mathbf{q} = 0.48\,\mathbf{c}^*$. This modulation as well as the **q** wavevector distribution has been confirmed by electron diffraction. Experiments are in progress to address the lixiviation behavior and to correlate it to the occurrence of the amorphous phase. This study, as all those reported in literature and related to hollandite materials with closed composition, shows the high compound flexibility to adapt its structure to its chemical composition, as well in term of modulation as in term of a possible monoclinic distortion.

## Acknowledgment

The authors thank CEA and GDR NOMADE for their financial support.

## References

[1] G. Leturcq, F. Bart, A. Comte, Patent no EN, 01/15972, France, 2001.
[2] A.E. Ringwood, V.M. Oversby, S.E. Kesson, W. Sinclair, N. Ware, W. Hibberson, A. Major, Nucl. Chem. Waste Manage. 2 (1981) 287.
[3] S.E. Kesson, Radioactive Waste Manage. Nucl. Fuel Cycle 4 (1983) 53.
[4] A.Y. Leinekugel-le-Cocq-Errien, P. Deniard, S. Jobic, R. Cerny, F. Bart, H.J. Emerich, Solid State Chem. 179 (2006) 3197.
[5] J. Rodriguez-Carvajal, Laboratoire Léon Brillouin (CEA-CNRS), France, March 2002.
[6] A.G. De La Torre, S. Bruque, M.A.G. Aranda, J. Appl. Cryst. 34 (2001) 192.
[7] X. Orlhac, C. Fillet, P. Deniard, A.M. Dulac, R. Brec, J. Appl. Cryst. 34 (2001) 114.
[8] G.W. Brindley, Phil. Mag. 36 (1945) 347.
[9] P. Stadelmann, CIME-EPFL, CH-1015 Lausanne, 2001.
[10] A. Byström, A.M. Byström, Acta Cryst. 3 (1950) 146.
[11] D.S. Filimonov, Z.-K. Liu, C.A. Randall, Mat. Res. Bull. 37 (2002) 2373.
[12] H. Leligny, Ph. Labbé, M. Ledésert, B. Raveau, Acta Cryst. B48 (1992) 134.
[13] M.L. Carter, R.L. Withers, J. Solid State Chem. 178 (2005) 1903.
[14] R.W. Cheary, Acta Cryst. B42 (1986) 229.
[15] R.W. Cheary, R. Squadrito, Acta Cryst. B45 (1989) 205.
[16] N.B. Bolotina, M.T. Dmitrieva, R.K. Rastsvetaeva, Sov. Phys. Crystallogr. 37 (3) (1992) 311.
[17] R.W. Cheary, R. Squadrito, Acta Cryst. A48 (1992) 15.
[18] F. Bart, G. Leturcq, H. Rabiller, Ceram. Trans. 168 (2005) 217.
[19] R.W. Cheary, A. Coelho, J. Appl. Cryst. 25 (1992) 109.
[20] T. IDA, Rigaku J. 19 (2002) 47.
[21] R.W. Cheary, A. Coelho, CCP14 Powder diffraction library, Engineering and Physical Sciences Research Council, Darsbury Laboratory, Warrington, England, 1996.
[22] V. Aubin-Chevaldonnet, M. Evain, A. YsolineLeinekugel-Le-Cocq-Errien, P. Deniard, S. Jobic, D. Caurant, V. Petricek, in preparation.
[23] F.C. Mijlhoff, D.J.W. Ijdo, H.W. Zandbergen, Acta Cryst. B41 (1985) 98.
[24] H.W. Zandbergen, P.L.A. Everstijn, F.C. Mijlhoff, G.H. Renes, D.J.W. Ijdo, Mat. Res. Bull. 22 (1987) 431.
[25] S.E. Kesson, T.J. White, Proc. R. Soc. Lond. A405 (1986) 73.
[26] S.E. Kesson, T.J. White, Proc. R. Soc. Lond. A408 (1986) 295.